RESEARCH ARTICLE

PROTEIN TARGETING

Mechanism of signal sequence handover from NAC to SRP on ribosomes during ER-protein targeting

Ahmad Jomaa[1]†, Martin Gamerdinger[2]†, Hao-Hsuan Hsieh[3]†, Annalena Wallisch[2], Viswanathan Chandrasekaran[4], Zeynel Ulusoy[2], Alain Scaiola[1], Ramanujan S. Hegde[4], Shu-ou Shan[3]*, Nenad Ban[1]*, Elke Deuerling[2]*

The nascent polypeptide–associated complex (NAC) interacts with newly synthesized proteins at the ribosomal tunnel exit and competes with the signal recognition particle (SRP) to prevent mistargeting of cytosolic and mitochondrial polypeptides to the endoplasmic reticulum (ER). How NAC antagonizes SRP and how this is overcome by ER targeting signals are unknown. Here, we found that NAC uses two domains with opposing effects to control SRP access. The core globular domain prevented SRP from binding to signal-less ribosomes, whereas a flexibly attached domain transiently captured SRP to permit scanning of nascent chains. The emergence of an ER-targeting signal destabilized NAC's globular domain and facilitated SRP access to the nascent chain. These findings elucidate how NAC hands over the signal sequence to SRP and imparts specificity of protein localization.

Localization of nascent proteins to the appropriate organelle is essential for cell function and homeostasis. The accuracy of cotranslational targeting to the endoplasmic reticulum (ER) relies on two ribosome-binding factors. Signal recognition particle (SRP) uses its M domain to engage hydrophobic ER-targeting signals as they emerge from the ribosomal tunnel and delivers the ribosome-nascent chain complex (RNC) to the SRP receptor (SR) at the ER membrane using its GTPase (NG) domain (*1*–*4*). SRP is far less abundant than ribosomes in the cell and has high affinity for all ribosomes. Thus, its access must be regulated to selectively target ribosomes displaying the ER signal sequence (*5*–*7*). The nascent polypeptide–associated complex (NAC) (composed of NACα and NACβ) prevents SRP from promiscuously targeting ribosomes without an ER-targeting signal (*8*–*12*). NAC consists of a central globular domain from which flexible N- and C-terminal tails extend (*13*–*15*). Cross-linking studies have suggested that the N-terminal tails are used for a range of interactions and participate in ribosome binding (*16*, *17*). The function of the C-terminal tails, including a conserved ubiquitin-associated domain (UBA) in NACα, is unknown. NAC and SRP share overlapping ribosome-binding sites, which may give rise to their antagonism (*16*). However, biochemical experiments have shown that NAC and SRP bind simultaneously to RNCs translating ER proteins (*9*, *11*, *12*), suggesting that there is a handoff intermediate in the poorly understood NAC-to-SRP exchange reaction. Thus, we set out to explain how NAC binds the ribosome to prevent SRP access and how this inhibition is preferentially overcome for ER-targeting signals.

[1]Department of Biology, Institute of Molecular Biology and Biophysics, ETH Zurich, 8093 Zurich, Switzerland. [2]Department of Biology, Molecular Microbiology, University of Konstanz, 78457 Konstanz, Germany. [3]Division of Chemistry and Chemical Engineering, California Institute of Technology, Pasadena, CA 91125, USA. [4]MRC Laboratory of Molecular Biology, Cambridge, UK.
*Corresponding author. Email: elke.deuerling@uni-konstanz.de (E.D.); ban@mol.biol.ethz.ch (N.B.); sshan@caltech.edu (S.S.)
†These authors contributed equally to this work.

Structures of NAC in complex with translating ribosome

We reconstituted in vitro a reaction with signal-containing RNC (RNC_{SS}) mixed with both NAC and SRP and analyzed the complexes formed using cryo–electron microscopy (cryo-EM) (fig. S1). This reaction was likely to contain intermediates at critical steps of cargo recognition and handover, which could be deconvoluted by in silico classification. We resolved two complexes within the particles, a pre-cargo handover RNCss•NAC complex, which we will discuss first, and a ternary post-cargo handover RNCss•NAC•SRP complex, which is discussed later.

The structure of the RNC_{SS}•NAC complex was similar to the RNC•NAC structure obtained from reanalysis of an RNC intermediate during translation of the cytosolic protein tubulin (TUBB) (figs. S2 and S3), on which NAC copurified (*18*). This suggests that NAC initially engages both signal-containing and signal-lacking RNCs but would be expected to hand over to SRP only in the presence of an ER signal sequence.

The structure of the RNCss•NAC complex (Fig. 1, A to D and G) revealed the interactions between the N-terminal tail of NACβ and the ribosome at 3.5 Å resolution (Fig. 1C and fig. S4). The tail, containing an RRKKK motif, formed an α-helix followed by a loop in an anchor-shaped turn wrapping around eL22 while also contacting eL19 and the ribosomal RNA (rRNA) (Fig. 1C and fig. S4). The structure rationalizes the key role of this domain in ribosome binding established previously (*16*, *17*, *19*). To validate the role of this tail as an anchor to the ribosome, we measured NAC-ribosome binding affinity using Förster resonance energy transfer (FRET) between a donor dye placed near the signal sequence on the nascent chain and an acceptor dye placed on NAC. Point mutations of the NAC tail weakened NAC-RNC binding by 10- to 40-fold (Fig. 1, E and F), consistent with its important role in ribosome binding.

The globular domain of NAC was resolved to ~8 Å resolution, which allowed rigid-body fitting of an AlphaFold-predicted structure (*20*) (Fig. 1, A and B, and fig. S5). On the basis of this interpretation, two positively charged α-helices contributed by both NAC subunits contacted rRNA on the surface of the ribosome (Fig. 1G and fig. S5). Charge reversal mutations of a positively charged residue in each helix (K78E-NACα or K43E-NACβ) weakened ribosome binding of NAC in vitro (fig. S6A) and in vivo (fig. S6B).

The binding site of the NAC globular domain overlapped with that of the SRP M domain and was mutually exclusive with SRP binding (Fig. 1G and fig. S6C) (*3*, *4*), consistent with a low-resolution cryo-EM map of NAC in complex with inactive ribosomes (*16*). This finding suggests that NAC interaction at the ribosome exit site is the basis of SRP inhibition. In agreement with this hypothesis, a ribosome-binding mutant in the globular domain (K78E-NACα combined with K43E-NACβ, named NAC KK-EE) was impaired in its ability to compete with SRP binding in vitro (Fig. 1H). The residual binding of NAC KK-EE to the ribosome is likely mediated by the N terminus of NACβ, the position of which would not interfere with SRP binding (fig. S6C).

The corresponding NAC KK-EE mutations in *Caenorhabditis elegans* showed reduced competition of SRP binding by NAC, as shown by elevated levels of ribosome-bound SRP (Fig. 1I and fig. S6D), as well as increased recovery of mRNAs coding for non-ER proteins in SRP pull-downs (fig. S6E). The reduction in SRP competition correlated with elevated levels of a green fluorescent protein (GFP) reporter of ER stress driven by the hsp-4 promoter (hsp-4p::GFP) (*21*), particularly in highly secretory intestinal cells (fig. S6F). Moreover, worms expressing mutant NAC showed reduced embryonic viability (fig. S6G) and a shortened adult life span (fig. S6H).

NAC is destabilized by ER signal sequences, allowing access of SRP to the ribosome exit

SRP antagonism by NAC must be relieved when an ER-targeting signal emerges from the ribosome. One possible explanation for this is that

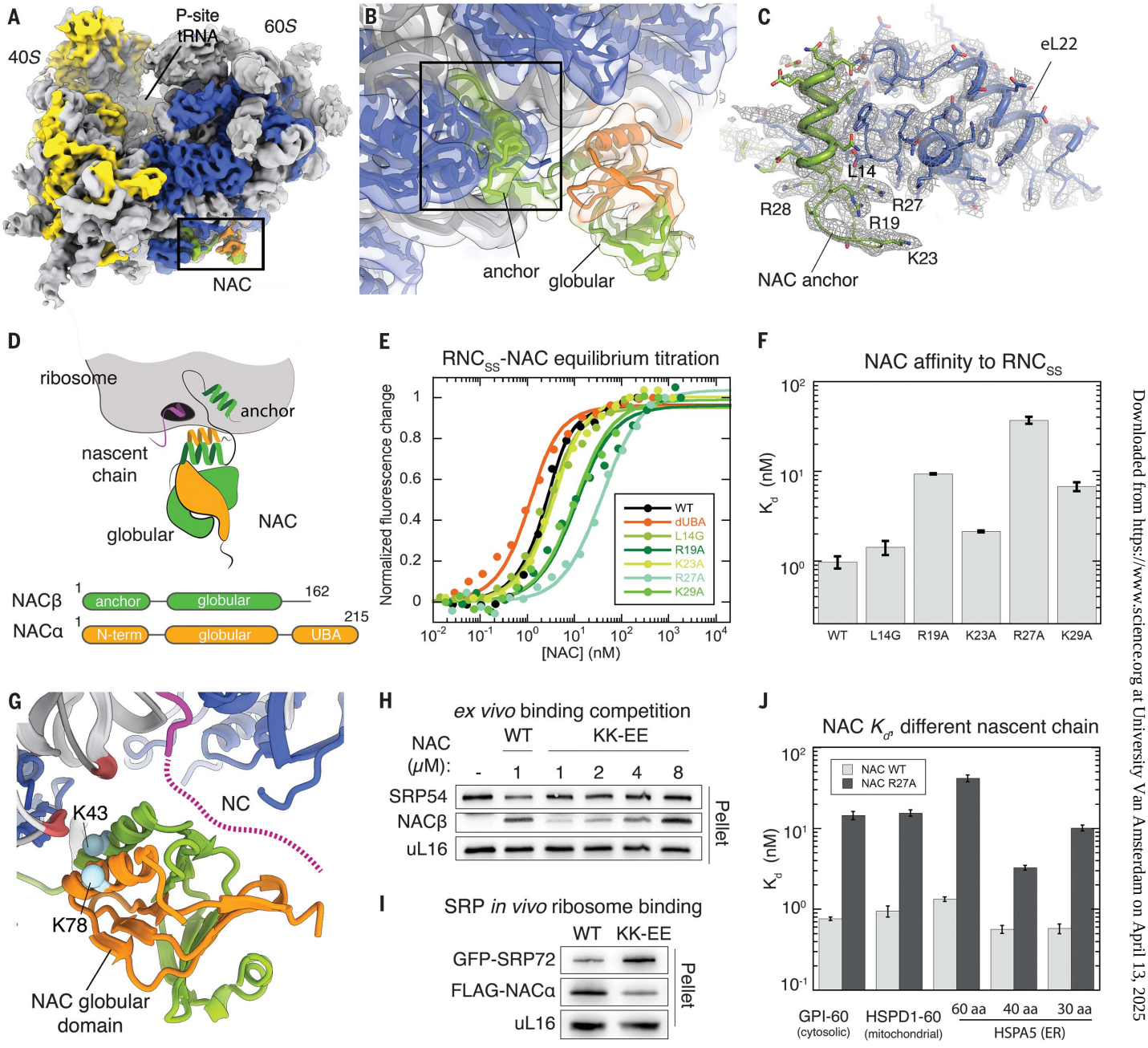

Fig. 1. Structure of the ribosome•NAC complex reveals interactions between the NAC globular and anchor domains with the nascent chain and the ribosome. (**A**) Cryo-EM structure of the RNCss•NAC complex. Boxed region indicates the magnified region shown in (B). (**B**) Closeup of the ribosome tunnel exit region. NACβ is colored green and NACα is colored orange. Anchor and globular domains of NAC are indicated. (**C**) Closeup of the N terminus of NACβ fitted into cryo-EM densities shown as mesh. Ribosomal protein eL22 is shown as a blue cartoon ribbon. (**D**) Schematic of the RNC•NAC complex with a domain structure of NAC. (**E**) Equilibrium titrations to measure the binding of the indicated NAC mutants to RNC_{SS}. The fluorescence signal changes were normalized to the end point of each titration for comparison. The lines are fits of the data to Equation 2. (**F**) Summary of the dissociation constant (K_d) values from (E). (**G**) Closeup of the NAC globular domain highlighting the two antiparallel α-helices, with residues K78 (NACα) and K43 (NACβ) shown as spheres (blue) interacting with the backbone of the rRNA (red). Dashed line indicates the flexible nascent chain (NC, magenta). (**H**) Crude cellular RNCs were incubated with purified NAC proteins and pelleted by sucrose cushion centrifugation. Proteins were detected by immunoblotting. (**I**) Sucrose cushion centrifugation of ribosomes in *C. elegans* expressing the indicated NAC variants and GFP-tagged SRP72. Proteins in the pellet fraction were detected by immunoblotting. (**J**) Summary of the K_d values of NAC R27A for RNCs displaying the nascent chains of GPI (cytosolic), HSPD1 (mitochondrial), and HSPA5 (ER) at the indicated nascent chain lengths. K_d values were from analysis of the data shown in fig. S8, C and D. Error bars are covariances of the fitted K_d values.

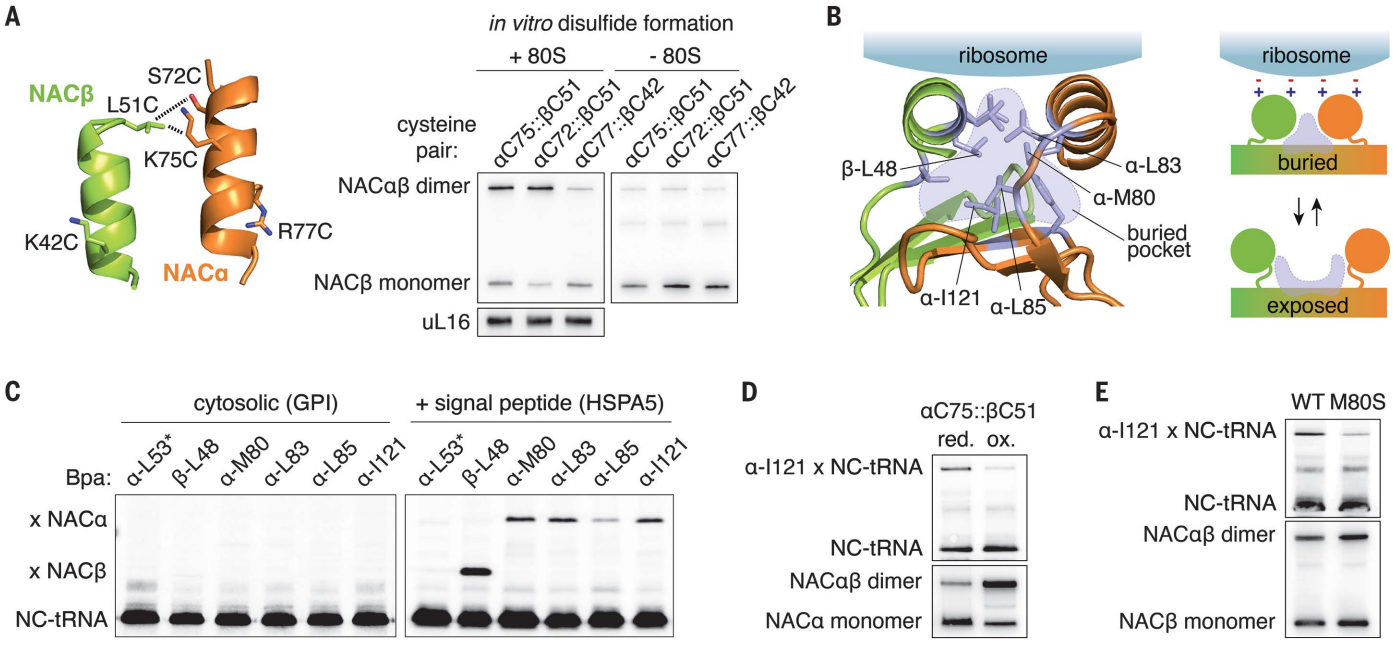

Fig. 2. ER signal sequences are sensed by the ribosome-binding helices of NAC. (**A**) NAC's ribosome-binding helices showing the positions of pairwise cysteine mutants tested for disulfide bond formation. Side chains shown are based on AlphaFold prediction. Dashed lines indicate pairs sufficiently close to form a disulfide bond revealed by immunoblotting (right panel) in the presence of inactive 80*S* ribosomes. (**B**) Residues contributing to the hydrophobic pocket between the two α-helices of NAC (purple). The right side shows a model where ribosome dissociation leads to separation of the helices, thereby exposing a hydrophobic pocket. (**C**) Autoradiograph of photo-cross-linking of Bpa-NAC variants to stalled RNCs carrying 50–amino acid S^{35}-labeled nascent chains of cytosolic GPI (left) or a GPI fusion protein containing the N-terminal signal peptide of HSPA5 (right). The positions of the tRNA-attached nascent chain (NC-tRNA) and its cross-links to NACα and NACβ are indicated. Asterisk indicates a position outside the hydrophobic region. (**D**) Autoradiograph of photo-cross-linking of the αC75-βC51 cysteine variant carrying Bpa at α-I121 to HSPA5-RNCs (55 amino acids), performed in the reduced (red.) and oxidized (ox.) state. (**E**) Autoradiograph and immunoblotting of 55–amino acid HSPA5-RNC photo-cross-linking of the indicated α-I121 Bpa-NAC variants.

hydrophobic ER-targeting signals somehow weaken the interaction between the NAC globular domain and the ribosome to allow SRP access. To test this, we compared the affinity of NAC for RNCs displaying either an ER signal sequence (RNC_{SS}) or a mutated signal sequence that inhibits ER targeting (RNC_{SSmt}) (fig. S7) (*7*). Because the NACβ anchor tail would mask the affinity differences, we performed FRET measurements with NAC mutants with a disrupted RRKKK motif. These mutants, NAC-R27A and NAC-K29A, bound to RNC_{SS} with ~3.5-fold and ~5-fold weaker affinity, respectively, compared with RNC_{SSmt} (fig. S8, A and B).

We then measured NAC binding to purified RNCs bearing ER, cytosolic, and mitochondrial nascent chains (HSPA5, GPI, and HSPD1, respectively) stalled at residue 60, exposing short N-terminal sequences (~30 amino acids) at the tunnel exit (fig. S7). In agreement with our hypothesis, NAC R27A bound 5-fold more weakly to RNC_{HSPA5} exposing an ER signal sequence than to RNC_{GPI} and RNC_{HSPD1} (Fig. 1J and fig. S8, C and D).

We repeated the binding measurements with purified RNCs bearing an ER signal sequence at nascent chain lengths of 30, 40, and 60 amino acids (Fig. 1J and fig. S8, C and D). NAC showed the strongest interaction with the ribosome when the signal sequence was in the tunnel (30 and 40 amino acids), and binding was weakened by >10-fold when the ER signal peptide was exposed (60 amino acids). Thus, the emergence of a hydrophobic signal peptide, but not another type of nascent chain, weakens the interaction of the NAC globular domain with the ribosome.

We then investigated the role of the two ribosome-binding antiparallel helices that dock the globular domain on the ribosome in proximity to the emerging nascent chain. The helices are amphipathic and orient the positively charged side toward the ribosome surface, whereas the hydrophobic side contributes to a buried hydrophobic pocket (fig. S5). These helices were sensitive to proteolysis when human NAC was subjected to crystallization (*15*), suggesting that they are flexibly disposed in solution but are apparently stabilized in the ribosome-bound state. To test this, we engineered two cysteines in the helices such that they would be apposed to each other in the ribosome-bound NAC structure. Consistent with our hypothesis, the engineered cysteines formed a disulfide bond after oxidant treatment only in the presence of the ribosome (Fig. 2A and fig. S9).

To investigate whether the emergence of the signaling peptides may destabilize and release the globular domain of NAC from the ribosome (Fig. 2B), we incorporated photo-cross-linking probes both inside and outside the hydrophobic pocket (Fig. 2B) and tested their proximity to nascent chains coding for a cytosolic, mitochondrial, or ER protein. NAC variants carrying the probe within the hydrophobic pocket (e.g., NACα-I121) cross-linked to ER targeting signals (Fig. 2C and fig. S10, A to C). Cross-linking was dependent on nascent chain length and was only seen once the targeting signal was fully exposed outside the exit tunnel (fig. S10A). Cross-linking was prevented when the helices were covalently linked by disulfide bond formation, demonstrating that destabilization of the NAC globular domain by the ER signal peptide requires separation of the helices (Fig. 2D). Furthermore, cross-linking to the pocket residues NACα-I121 and NACβ-L48, but not the less buried NACα-M80, was modulated by changing targeting signal hydrophobicity (fig. S10D). Mutating M80 to serine impaired nascent chain photo-cross-linking to NACα-I121 (Fig. 2E), which suggests that this residue also contributes to nascent chain sensing.

These results indicate that an ER signal sequence destabilizes the NAC globular domain. The NACβ N-terminal tail remains anchored to the ribosomal surface regardless of the nascent

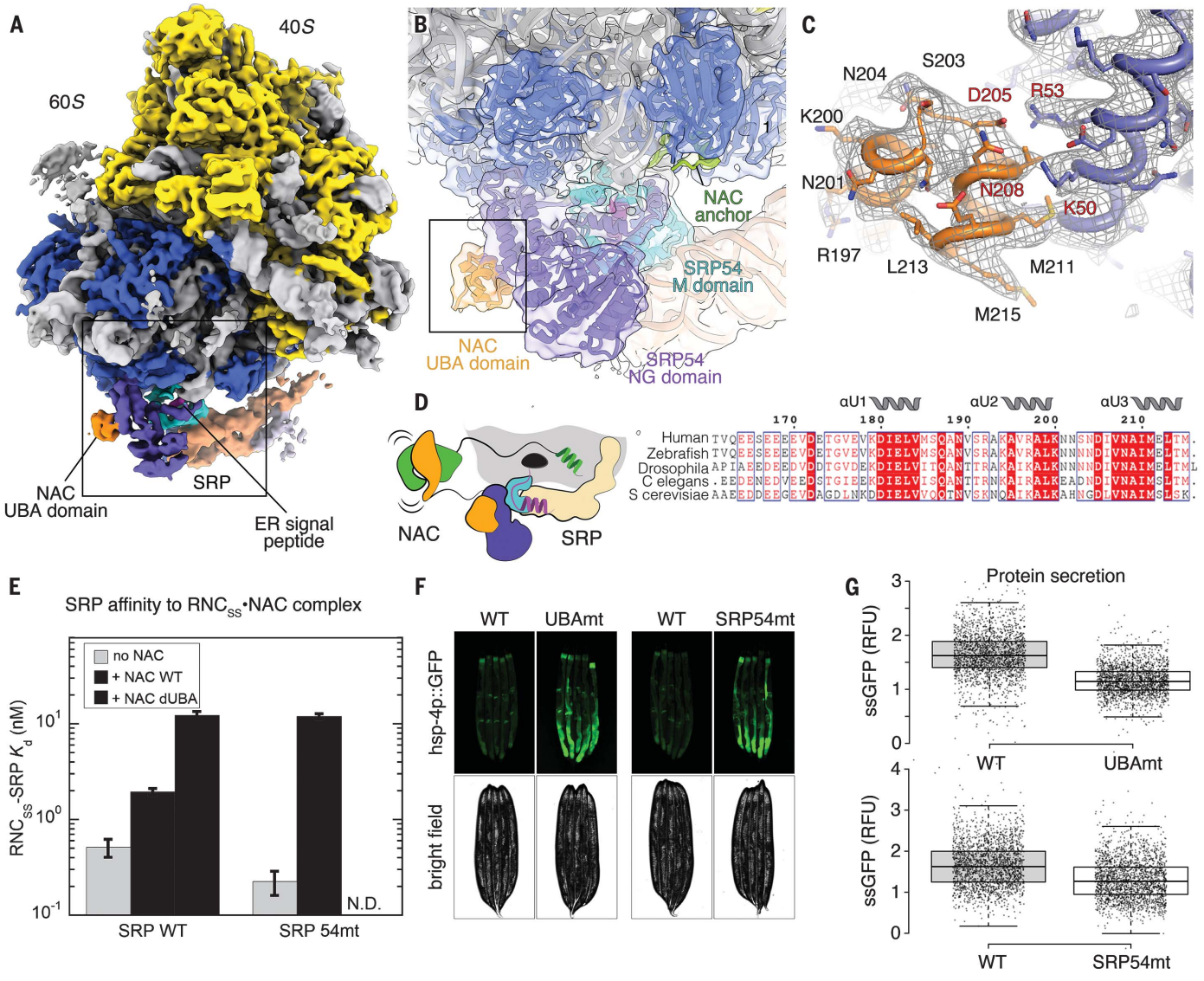

Fig. 3. Structure of the ribosome•SRP•NAC complex. (**A**) Cryo-EM structure of the RNCss•NAC•SRP complex. Boxed region indicates the closeup shown in (B). (**B**) Ribosome tunnel exit regions depicting the SRP54 NG and M domains, the NACα UBA domain, and the NACβ anchor domain are colored slate, cyan, orange, and green, respectively. Underlying EM density is shown as a transparent surface. (**C**) Closeup on the UBA interactions with SRP54 NG domain shown as cartoon and sticks, fitted into cryo-EM densities shown as mesh. (**D**) Schematic representation of the ternary complex. Boxed region shows sequence alignment of NACα UBA domain in eukaryotes. (**E**) Summary of the K_d values for the binding of wild-type and mutant SRPs to RNC$_{SS}$•NAC, based on fitting of the data in fig. S17A. N.D., not determined. (**F**) and (**G**) Fluorescence microscope images of hsp-4p::GFP worms (F) and worm flow cytometry analysis of ssGFP (G) in worms carrying the indicated RNA interference (RNAi)–resistant genes in the endogenous RNAi background. Box plot center line indicates the median, box length the upper and lower quartile, and whiskers the minimum/maximum quartile ($N \geq 2000$).

chain, as evidenced by cross-linking between a residue in the NACβ anchor and the ribosomal protein eL22, whereas a probe in the N terminus of NACα changed its location only for the ER substrate (fig. S11). Combined, these results suggest that NAC interactions with the ribosome are remodeled as the signal peptide emerges from the ribosome tunnel.

Flexibly tethered UBA domain of NAC recruits SRP

The cryo-EM data on RNC$_{SS}$ mixed with both NAC and SRP also allowed us to visualize the complex with NAC and SRP simultaneously bound to the ribosome (RNCss•NAC•SRP) (Fig. 3A and figs. S1 and S12). The conformation of SRP in the ternary complex was similar to that of previously observed SRP-ribosome complexes (*3*, *4*). The density for the NACβ anchor was observed in a similar position as in the RNC•NAC complexes (fig. S12C). However, the globular domain of NAC was no longer resolved, because its binding position at the tunnel exit was occupied by the SRP54 M domain (Figs. 1G and 3, A to D).

In addition, we observed density for the flexibly tethered C-terminal UBA domain of NACα bound to the N domain of SRP54 (Fig. 3, B and C, and figs. S12 and S13). The interactions occupied two patches of contact points and involved a number of salt bridges and specific hydrogen bonds between highly conserved residues (Fig. 3, C and D, and fig. S14). The UBA-binding site on SRP54 overlapped with the binding site of the NG domain of SR (fig. S15), which suggests that formation of the SRP•SR complex will displace NAC from SRP at the ER membrane (*22*–*24*). The direct interaction of the UBA domain of NAC with SRP raises questions as to whether it plays a role in ER targeting.

To address this, we generated the following: (i) a NAC mutant in which the UBA is deleted (dUBA), (ii) a NAC mutant (D205R/N208R-NACα, named UBAmt), and (iii) an SRP mutant (K50E/R53E-SRP54, named SRP54mt on the basis of human sequence numbering). UBAmt and SRP54mt contain charge reversal mutations at contact points between the UBA and the NG domain of SRP54. We measured the effects of these mutations on the binding affinity of SRP for NAC-engaged RNC_{SS} displaying the ER signal sequence. Although none of the above-described mutations changed the affinity of NAC or SRP for SR or RNCs (figs. S16 and S17), they all decreased the affinity of SRP for the RNC_{SS}•NAC complex by >5-fold (Fig. 3E and fig. S17A). The same effect was observed in reciprocal experiments when NAC was titrated to a preformed RNC_{SS}•SRP complex (fig. S17, B and C). Thus, the contact between NAC UBA and SRP54 NG domains stabilizes the cobinding of SRP and NAC on signal sequence–displaying ribosomes.

To test whether the UBA domain mediates the initial recruitment of SRP to the ribosome, we used total internal reflection fluorescence microscopy to study single-molecule events in which SRP binds to surface-immobilized RNC_{SS} prebound with NAC (Fig. 4A). If SRP is captured by NAC through the UBA domain before stable engagement with the ribosome, then the arrival of SRP on NAC-bound RNC_{SS} would be synchronous with the onset of FRET between a dye pair engineered on the SRP54 NG and NACα UBA domains. The results were consistent with this model: The initiation of colocalized fluorescence signals from NAC and SRP was synchronous with the onset of FRET in every single-molecule fluorescence time trace (Fig. 4, B and C), even in recruitment events that did not lead to a long-lived SRP association with the RNC (for an example, see Fig. 4B). Statistical analysis, in which the FRET time traces were aligned to the start of the SRP fluorescence signal (n = 45), showed that peak FRET efficiency was coincident with SRP arrival (Fig. 4D). Once a stable RNC•NAC•SRP ternary complex was formed, NACα UBA dynamically associated with and dissociated from SRP54, as shown by the frequent transitions between low- and high-FRET states (Fig. 4E). Thus, the contact between UBA and NG initiates before the productive docking of SRP at the exit of the ribosomal tunnel and signal sequence handover.

C. elegans mutants with impaired NAC UBA-SRP54 NG interactions showed elevated levels of the ER stress reporter hsp-4p::GFP, particularly in highly secretory intestinal cells (Fig. 3F and fig. S18, A and B). Furthermore, the levels of a secreted GFP reporter containing a signal sequence (ssGFP) (*25*) were significantly lower in NAC UBA and SRP54 NG mutant worms (Fig. 3G and fig. S18, C and D). The mutant worms also showed a cytosolic stress response, suggesting a possible accumulation of misfolded ER proteins in the cytosol caused by failed targeting (fig. S18E). As mentioned above, the defects observed with SRP54mt were not caused by the impaired interaction with the SR NG domain (figs. S15 and S16). Thus, the contacts between SRP and the UBA domain of NAC are critical for the successful SRP targeting of proteins to the ER.

Mechanism of the NAC-SRP interplay on the ribosome to initiate ER targeting

We propose a molecular mechanism for the interplay of NAC and SRP at the ribosome that controls and initiates cotranslational protein targeting to ER: NAC acts as "gatekeeper" to shield emerging nascent chains from nonphysiological interactions with SRP (Fig. 5). Because of its abundance and high affinity for the ribosome, NAC is bound to most ribosomes at early stages of translation through a high-affinity anchor and a weakly bound globular domain that blocks SRP access to nascent polypeptides. The flexibly tethered UBA domain recruits SRP and increases its local concentration at the tunnel exit region to initiate sampling of nascent chains. The emergence of an

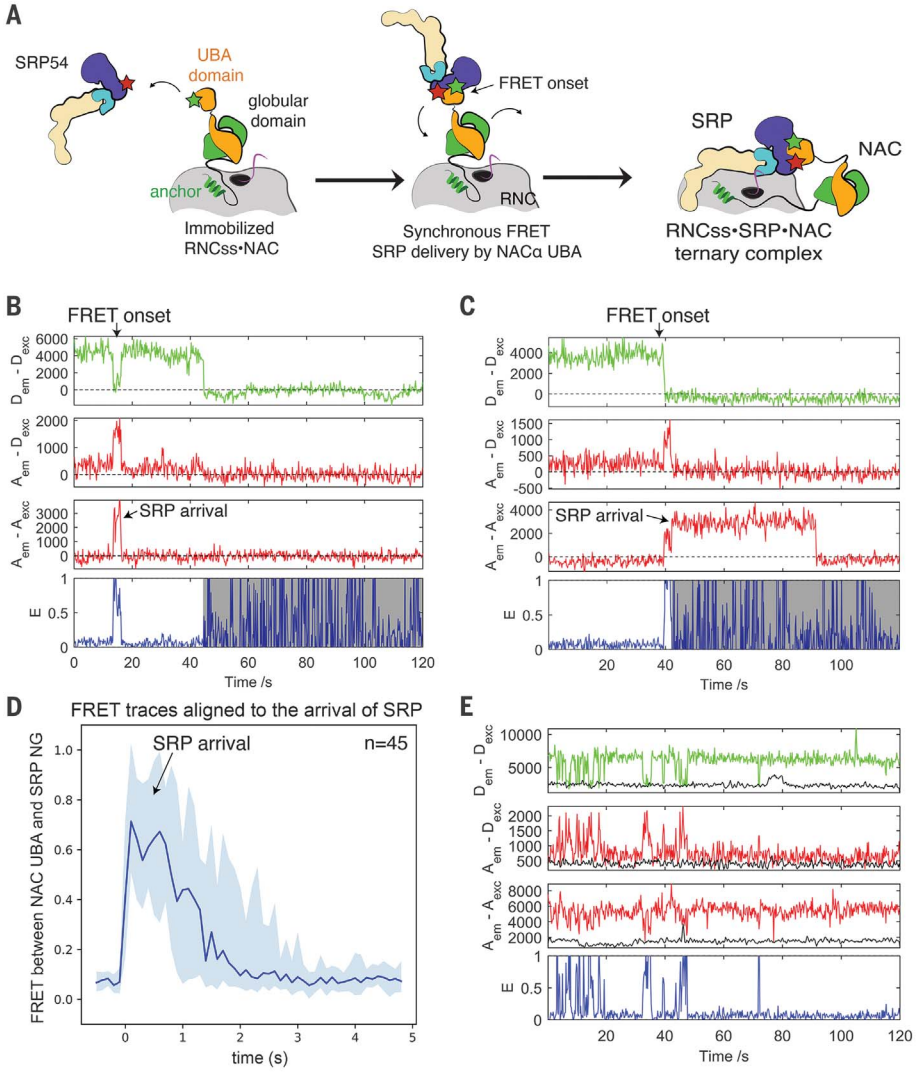

Fig. 4. Interaction between SRP54 and NACα UBA domain mediates initial SRP recruitment to the ribosome. (**A**) Scheme of the single-molecule experiment. RNC is immobilized on the glass coverslip surface through 3′ biotinylated mRNA (not shown). NAC was labeled with Cy3b (green star) in the UBA domain, and SRP is labeled with Atto647N (red star) in the SRP54 NG domain. (**B**) and (**C**) Representative single-molecule fluorescence time traces. $D_{em} - D_{ex}$, donor emission during donor excitation; $A_{em} - D_{ex}$, acceptor emission during donor excitation; $A_{em} - A_{ex}$, acceptor emission during acceptor excitation; and E, apparent FRET efficiency calculated from the $A_{em} - D_{ex}$ and $D_{em} - D_{ex}$ traces. The region after donor photobleaching is masked. (**D**) Time traces of FRET efficiency (n = 45) aligned to the start of the SRP (acceptor) signal. The median FRET value of all traces at each time frame is plotted as a solid blue line. The blue shaded area encloses the FRET range that includes the first to third quartile of data at each frame. (**E**) Representative time trace after a stable NAC•SRP•RNC ternary complex is formed.

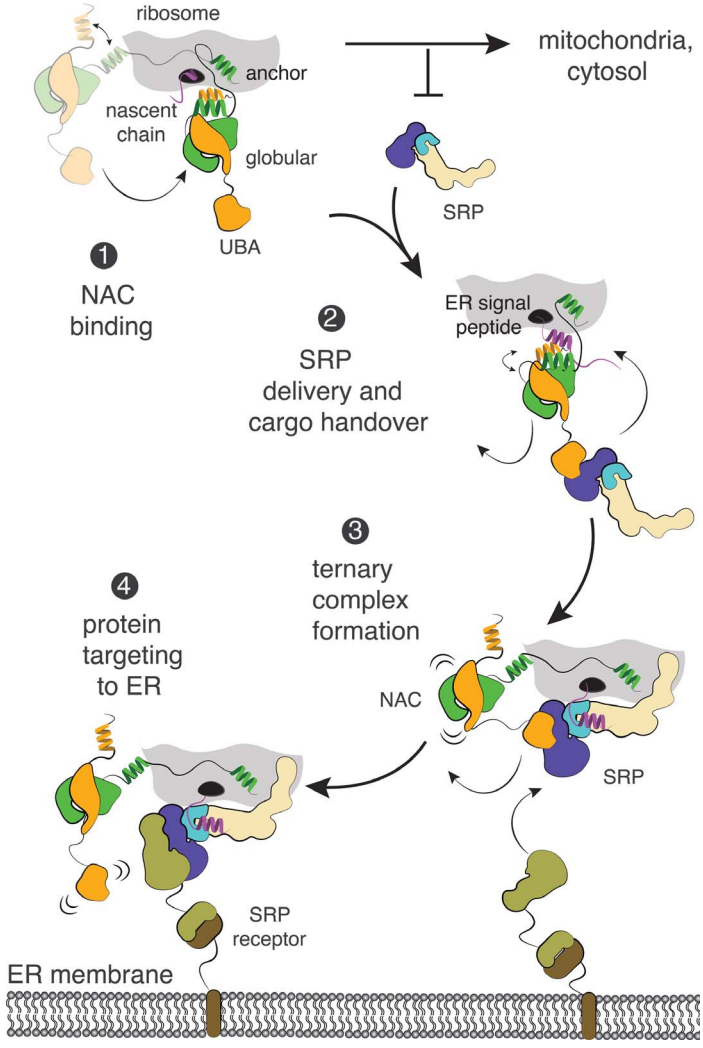

Fig. 5. Model for cotranslational signal sequence handover from NAC to SRP during ER-protein targeting.

ER signal sequence weakens the interactions of NAC's globular domain with the ribosome. This allows SRP to bind the signal sequence at the exit of the ribosomal tunnel, displacing the globular domain of NAC. NAC remains associated with both the ribosome and SRP through the respective NACβ anchor and UBA contacts until it reaches the ER membrane, where SR displaces the UBA domain from SRP.

This study resolves the molecular function of NAC as a sorting factor for nascent chains and the nature of its spatiotemporal coordination with SRP on the ribosome. Our results explain how NAC, which binds to virtually all ribosomes, prevents sub-stoichiometric SRP from forming tight but unproductive complexes with signal-less ribosomes while at the same time keeping SRP tethered to allow it to scan for the presence of the ER signal sequence. Because degenerate and highly diverse targeting sequences cannot be recognized with sufficient specificity in a single step and/or by individual targeting factors, stepwise recognition by NAC followed by SRP, coupled with quality control pathways (*26*–*29*), increases the overall fidelity of protein targeting. The exit region of the ribosomal tunnel is a crowded environment where multiple binding factors compete for the nascent chain. Therefore, it is possible that NAC's role as a sorting factor extends beyond the recruitment of SRP to orchestrate a multitude of nascent chain–processing events.

REFERENCES AND NOTES

1. R. Gilmore, G. Blobel, P. Walter, *J. Cell Biol.* **95**, 463–469 (1982).
2. M. Halic *et al.*, *Nature* **444**, 507–511 (2006).
3. R. M. Voorhees, R. S. Hegde, *eLife* **4**, e07975 (2015).
4. A. Jomaa *et al.*, *Cell Rep.* **36**, 109350 (2021).
5. E. A. Costa, K. Subramanian, J. Nunnari, J. S. Weissman, *Science* **359**, 689–692 (2018).
6. M. Gamerdinger, M. A. Hanebuth, T. Frickey, E. Deuerling, *Science* **348**, 201–207 (2015).
7. J. H. Lee *et al.*, *Proc. Natl. Acad. Sci. U.S.A.* **115**, E5487–E5496 (2018).
8. B. Wiedmann, H. Sakai, T. A. Davis, M. Wiedmann, *Nature* **370**, 434–440 (1994).
9. M. del Alamo *et al.*, *PLOS Biol.* **9**, e1001100 (2011).
10. Y. Nyathi, M. R. Pool, *J. Cell Biol.* **210**, 287–301 (2015).
11. Y. Zhang *et al.*, *Mol. Biol. Cell* **23**, 3027–3040 (2012).
12. H.-H. Hsieh, J. H. Lee, S. Chandrasekar, S. O. Shan, *Nat. Commun.* **11**, 5840 (2020).
13. Y. Liu, Y. Hu, X. Li, L. Niu, M. Teng, *Biochemistry* **49**, 2890–2896 (2010).
14. L. Wang *et al.*, *Protein Cell* **1**, 406–416 (2010).
15. T. Spreter, M. Pech, B. Beatrix, *J. Biol. Chem.* **280**, 15849–15854 (2005).
16. M. Gamerdinger *et al.*, *Mol. Cell* **75**, 996–1006.e8 (2019).
17. R. D. Wegrzyn *et al.*, *J. Biol. Chem.* **281**, 2847–2857 (2006).
18. Z. Lin *et al.*, *Science* **367**, 100–104 (2020).
19. M. Pech, T. Spreter, R. Beckmann, B. Beatrix, *J. Biol. Chem.* **285**, 19679–19687 (2010).
20. J. Jumper *et al.*, *Nature* **596**, 583–589 (2021).
21. M. Calfon *et al.*, *Nature* **415**, 92–96 (2002).
22. K. Wild *et al.*, *J. Mol. Biol.* **428**, 2880–2897 (2016).
23. J. H. Lee *et al.*, *Sci. Adv.* **7**, eabg0942 (2021).
24. K. Kobayashi *et al.*, *Science* **360**, 323–327 (2018).
25. H. Fares, I. Greenwald, *Nat. Genet.* **28**, 64–68 (2001).
26. Y. C. Chen *et al.*, *EMBO J.* **33**, 1548–1564 (2014).
27. R. S. Hegde, E. Zavodszky, *Cold Spring Harb. Perspect. Biol.* **11**, a033902 (2019).
28. T. Hessa *et al.*, *Nature* **475**, 394–397 (2011).
29. V. Okreglak, P. Walter, *Proc. Natl. Acad. Sci. U.S.A.* **111**, 8019–8024 (2014).

ACKNOWLEDGMENTS

We thank M. Leibundgut, T. Lenarcic, and M. Jaskolowski for discussions; R. Schloemer and E. Coellen for technical assistance; and S. Kreft for help with in vitro cysteine cross-linking experiments. Cryo-EM was collected at ScopeM at the ETH Zurich. We acknowledge the MRC - LMB Electron Microscopy Facility for access and support of electron microscopy sample preparation and data collection for NAC-TTC5-RNC and the Caenorhabditis Genetics Center for strains. **Funding:** This work was supported by the Swiss National Science Foundation (grant no. 310030B_163478); the National Center of Excellence in Research RNA & Disease Program of the SNSF (grant no. 51NF40_141735); a Roessler Prize, Ernst Jung Prize, and Otto Naegeli Prize for Medical Research (to N.B.); the German Science Foundation (grant nos. SFB969/A01 and A07 to E.D. and M.G.); the National Institutes of Health (grant no. R35 GM136321 to S.S.); the National Science Foundation (grant no. MCB-1929452 to S.-o.S); and the UK Medical Research Council (MRC grant MC_UP_A022_1007 to R.S.H.). V.C. was supported by V. Ramakrishnan, whose funding was from the MRC (grant no. MC_U105184332), the Wellcome Trust (grant no. WT096570), the Agouron Institute, and the Louis-Jeantet Foundation. We also acknowledge the support of the NVIDIA Corporation for the Titan Xp GPU through a grant awarded to A.J. **Author contributions:** A.J., M.G., H.-H.H., R.S.H., S.S., N.B., and E.D. conceived the project. A.J. and A.S. performed cryo-EM data collection for ER-targeting complexes containing NAC and SRP. A.J. determined the cryo-EM structures of NAC-RNC and NAC-SRP-RNC. M.G. and A.W. performed *C. elegans* in vivo and A.W. cross-linking experiments. H.-H.H. performed FRET titrations and single-molecule experiments. V.C. performed structural analysis of the NAC-TTC5-RNC. Z.U. characterized NAC cysteine variants. A.J., M.G., H.-H.H., S.S., E.D., and N.B. wrote the manuscript. All authors contributed to data analysis and the final version of the manuscript. **Competing interests:** The authors declare no competing interests. **Data and materials availability:** Cryo-EM maps and model coordinates are deposited in the EMDB as EMD-14191, EMD-14192, and EMD-14193 and in the PDB as PDB ID 7QWQ, 7QWR, and 7QWS for the NAC-SRP-RNC$_{SS}$, NAC-RNC$_{SS}$, and NAC-TTC5-RNC$_{TUBE}$, respectively. All other data are available in the main text or the supplementary materials.

SUPPLEMENTARY MATERIALS

science.org/doi/10.1126/science.abl6459
Materials and Methods
Figs. S1 to S18
Tables S1 to S3
References (*30*–*42*)
MDAR Reproducibility Checklist

View/request a protocol for this paper from *Bio-protocol*.

27 July 2021; resubmitted 3 December 2021
Accepted 27 January 2022
10.1126/science.abl6459